ADVANCED SENSOR RESEARCH Open Access
www.advsensorres.com

Noise Spectroscopy of Liquid–Solid Interface Processes in Adjusted Physiological Solutions Using GAA Si Nanowire FET Biosensors

*Yongqiang Zhang, Nazarii Boichuk, Denys Pustovyi, Hanlin Long, Valeriia Chekubasheva, Mykhailo Petrychuk, and Svetlana Vitusevich**

Liquid gate-all-around (LGAA) field-effect transistor (FET) biosensors represent advanced material device structures responding electrically to surface potential change and allowing ultra-high sensitivity to biochemical liquids and human bodily fluids. However, the origin and physical working mechanisms for such a type of signals in different complex biochemical solutions remain still many opened questions. Here, noise spectroscopy and impedance methods are applied to study liquid–solid interface properties in LGAA FETs working in adjusted physiological solutions of different pH values. High-quality liquid LGAA Si nanowire (NW) FET biosensors demonstrate the high electronic performance of *I–V* characteristics in good agreement with modeling data. Impedance spectroscopy measurements allow for analyzing the double-layer capacitances and ion behavior under different pH conditions. Moreover, the noise spectra of the current fluctuations in the biosensors for several solutions are analyzed at different applied liquid-gate and drain-source voltages. The results demonstrate accurate detection of the dynamic ion processes on the nanowire surface. Charge inversion effect is revealed in single-valent ion solutions. Tiny signal characterization results obtained using the LGAA NW FET biosensors provide broader insights into the optimization of sensor parameters for biomedical molecular detection.

1. Introduction

With increasing demand for biomedical technology, biosensors with fast and sensitive signal responses are urgently required for various biological and medical applications. Liquid gate-all-around (LGAA) Si nanowire (NW) field-effect transistor (FET) biosensors have attracted considerable research attention due to their low cost, fast response, and high-speed sampling in addition to their low power consumption and label-free detection.[1] With the shrinking of the NW dimension and the enlargement of the surface-to-volume ratio, changes of charge carriers become significant and can be utilized as a detected electronic signal,[2] which is important for the precise detection of biomolecules. With surface functionalization using different biomolecular protocols, the detection of complex diseases can be achieved by analyzing small electronic signals.[3–5] However, it is difficult to assess the origin of dynamic processes at the liquid–solid interface for a device structure in contact with liquids of different properties to shed light on the real dynamics at the liquid–solid interface. Many efforts have been made to enhance the sensitivity of Si NW FETs, such as biomolecule immobilization,[6] surface modification,[3] and optimization of the NW FET structure.[7] Low-frequency noise was previously considered to be a hindrance caused by the carrier-trapping behavior in the dielectric layer covering the NW FET.[8,9] However, when the size of the NW decreases to the nano level, low-frequency noise can be used as a signal, since the electronic signal is determined by the single-trap phenomena (STP),[10,11] which are very sensitive to molecular concentrations at the liquid–solid interface.

Moreover, low-frequency noise can be applied as a powerful method for precise biomolecule signal detection and analysis. Noise spectroscopy data can be extracted from the measured power spectral density of the current fluctuations in the NW FET devices. In the case of the metal gate, the flicker noise can be analyzed for the trap density due to the contribution of numer-

Y. Zhang, N. Boichuk, D. Pustovyi, H. Long, V. Chekubasheva, M. Petrychuk, S. Vitusevich
Institute of Biological Information Processing (IBI-3)
Forschungszentrum Jülich
Jülich 52425, Germany
E-mail: s.vitusevich@fz-juelich.de
Y. Zhang, N. Boichuk, D. Pustovyi, S. Vitusevich
Experimentelle Physik 2
Technische Universität Dortmund
Dortmund 44227, Germany

The ORCID identification number(s) for the author(s) of this article can be found under https://doi.org/10.1002/adsr.202500101

DOI: 10.1002/adsr.202500101

ous traps near the NW interface. The appearance of flicker noise in the case of liquid-gated structures represents charge carrier trapping and emission processes influenced by the biological liquid in contact with the NW channel of the FET.[12] For the LGAA Si NW FET devices, the flicker noise behavior can thus reflect ion diffusion and transport processes, which can be regarded as useful information for the analysis of carrier behavior. Guo et al. revealed a space-charged-limited current effect and analyzed liquid–solid interface processes using *1/f* noise transformation to $1/f^{1.5}$ in an LG Si NW FET biosensor. The noise spectra characteristics in the low-frequency region reflect the ion process at the Si NW FET surface, which was demonstrated by the $MgCl_2$ ion response.[13] In addition, dimensionless Hooge parameters can be extracted from the noise spectrum, which are used for the quantitative analysis of noise performance in NW devices. Hooge parameters representing FET device performance and detection limits[14] provide useful information for biosensor characterization.

Noise spectroscopy can be used to analyze liquid-gated biosensors due to its enhanced molecular sensitivity.[12] As the NW scale decreases, the trap quantity is severely reduced to a single-trap level. For a liquid-gated NW FET, the benefit of a nanoscale NW and a high surface-to-volume ratio enables rapid single-carrier trapping-emission activity and the easy detection of tiny variations. The noise spectroscopy method enables selective biomolecule and chemical signal detection.[15–17] It also allows enhanced sensitivity to various biochemical environments for Si NW FET devices.[12,18–19] opening prospects for predictable biomedical diagnostics of different diseases, including Alzheimer's one. Noise spectroscopy can be regarded as a powerful tool for carrier behavior analysis and transport process studies, as this method allows for extracting small signals demonstrating the dynamics of ions and molecules at the liquid–solid interface. This method provides advantages for understanding the nanoelectric transformation of small molecular signals in solutions of different pH. For example, when pH of body fluid decreases from 6.9 to 6.5, living cells are destroyed and a tumor is formed.[20] In this respect, noise spectroscopy characterization of LGAA NW FETs in different liquid environments may provide in-depth insights into useful signal extraction in complex biomedical biosensor applications by selecting the optimal pH values of solutions or monitoring change of pH correlationg with impairing of human health.[21] It should be noted that noise spectroscopy and Hooge parameter analysis for physiological-like solutions of different pH values to find optimal regimes and sensor parameters for small biomedical signal detection are missing in the literature.

In this work, we applied noise spectroscopy to study LGAA NW FETs at different voltages in adjusted physiological solutions prepared based on phosphate-buffered saline (PBS) solutions of several pH values selected in the range close to that of the human body (pH 7.4). Low-frequency noise spectroscopy and impedance method measurements were used to study ion behavior in PBS with different pH strengths. We analyzed the noise signal behavior in liquid solutions by studying the spectral density of the current fluctuations and variation of double-layer capacitance at the liquid–solid interface. Our results demonstrate the good pH sensitivity of the LGAA Si NW FET device and the accurate detection of the dynamic processes, including the inversion effect of ions near the liquid–solid interface, promising for optimization of sensor parameters for small biological signal detection and analysis.

2. Results and Discussion

The LGAA Si NW FET structures were fabricated using a top-down approach over a low doping (10^{15} cm^{-3} doping concentration) silicon-on-insulator (SOI) wafer. A schematic presentation of the device structure in contact with a gate-all-around liquid and its influence on the NW channel is demonstrated in **Figure 1A**. We developed optimized technology to obtain high-quality liquid gate-all-around (LGAA) silicon nanowire (NW) field-effect transistors (FETs) with a nanowire length of 2 μm and a width of 150 nm. The doping concentration of the SOI wafer is 1×10^{15} cm^{-3}.The scanning electron microscope (SEM) image of the Si NW top view is shown in Figure 1B. The nanowires were formed by wet etching in a tetramethylammonium hydroxide (TMAH) solution, enabling an almost atomic-flat roughness of the NW surface. After the wet etching process, a 2-μm-long nanowire was formed. A cross-section of the GAA structure prepared for contact with a liquid gate environment during the measurement is shown in the SEM image in Figure 1C. From the cross-sectional view of the NW structure, a trapezoid nanowire with a top width of 100 nm and a bottom width of 200 nm can be characterized, and the nanowire cross-sectional image was obtained after using the focused ion beam cutting method. Good FET device performance can be demonstrated by measurements of transport and noise properties of the structures in different liquid solutions. Electrical measurements were performed in a 10 mM PBS of different pH values, while Si nanowires were covered by a 20-nm-thin SiO_2 protection layer to avoid direct contact with a liquid. PBS solutions were prepared using the Merck p4417 PBS tablet.[22] The gate voltage (V_{LG}) was controlled using an Ag/AgCl electrode in the liquid gate. Noise spectra were obtained for LGAA NW FETs in different solutions by applying the drain-source, $V_{DS,}$ and gate-source, V_{LG}, voltages.

First of all the *I–V* characteristics were studied in 10 mM PBS solutions of different pH values, ranging from 6.0 to 8.0 with an incremental increase of 0.2. Typical transfer characteristics (I_{DS}-V_{LG}) of LGAA NW FETs in different pH environments are shown in **Figure 2A**. Transfer curves reflect classic behavior for p^+-p-p+ FET device performance with a threshold voltage of ≈−0.4 V, which demonstrated the high quality of the NW FET structures obtained by the successful fabrication process. The pH-sensing property was also clearly demonstrated by the obvious shift (Figure 2B) in the transfer curve. To confirm good reproducibility to changes in pH values, measurements of transfer characteristics were performed several times in pH solutions with increased pH concentrations followed by the measurements in decreased pH concentrations. The results of repeated measurements in different pH sequences are shown in Figure S1 (Supporting Information). Using data from Figure 2B, the liquid gate voltage shift in solutions with a different pH can be studied. The change of liquid gate voltage revealed a linear dependence between the liquid gate voltage and the pH value at $I_{DS} = -200$ nA, with a resproducible response sensitivity of ≈17 mV/pH. The device also shows an obvious threshold voltage (V_{TH}) dependence

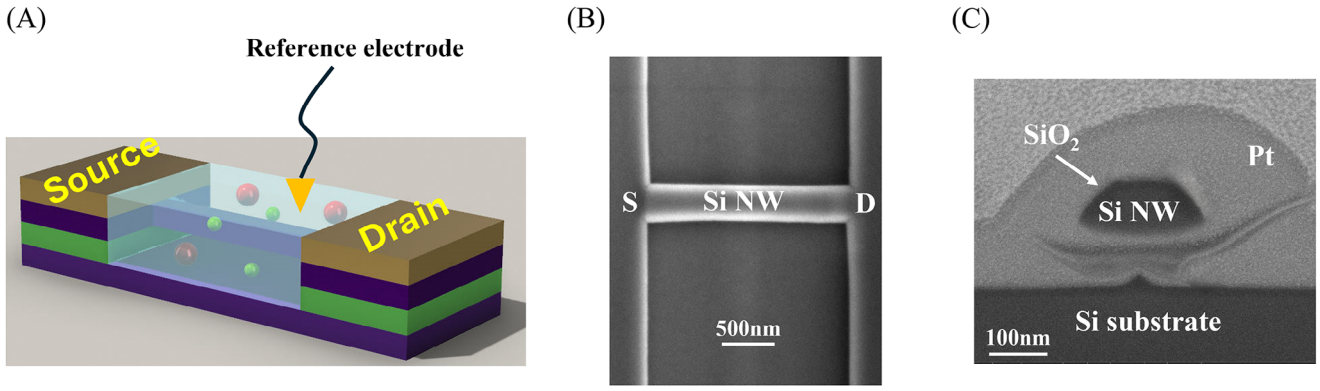

Figure 1. A) Schematic presentation of the LGAA Si NW FET device structure, where liquid surrounds the NW channel along the NW; B) scanning electron microscopy (SEM) image of the Si NW top view; C) SEM image of the cross-sectional view of the investigated GAA FET structure. Platinum, Pt, is the metallization layer utilized to perform the focused ion beam (FIB) cutting technique on one of the NW structures being tested.

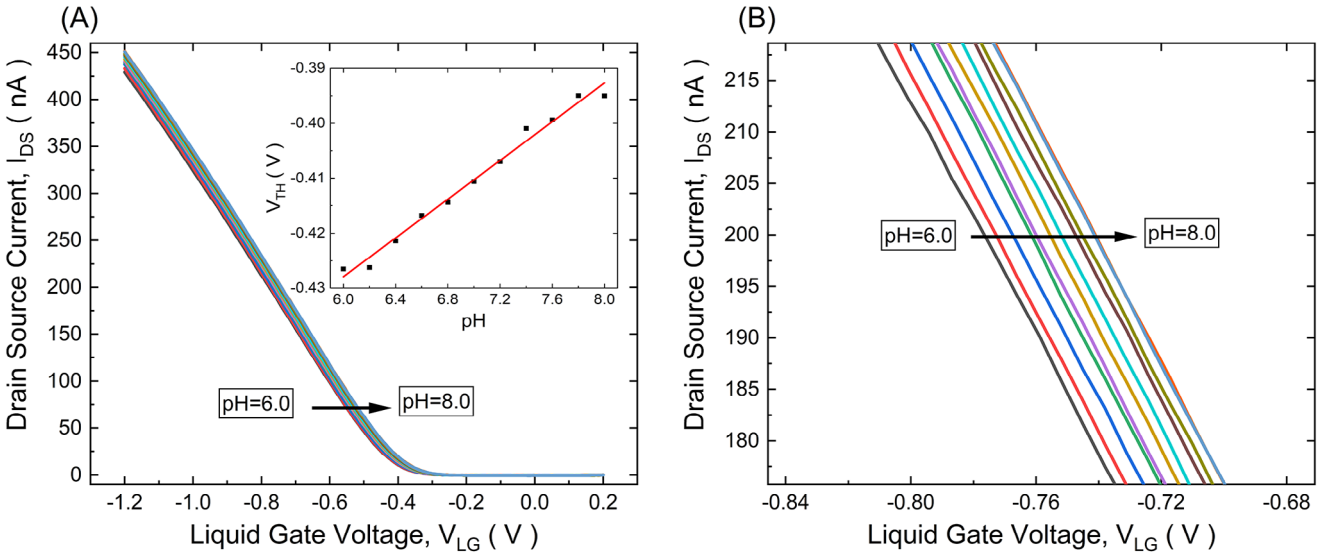

Figure 2. A) Typical transfer characteristics (I_{DS} – V_{LG}) of the LGAA NW FET at different pH values, with an incremental increase of pH in 0.2 pH step, reflecting 17mV/pH response at I_{DS} = 200 nA, obtained at V_{DS} = −0.1 V, Inset shows V_{TH} shift and linear fitting in solutions of different pH values; B) Enlarged region of *I–V* characteristic shown in Figure 1A, at I_{DS} = 200 nA, obtained at V_{DS} = −0.1 V.

on the pH change. Inset to Figure 2A shows the results of the V_{TH} changes as a function of different pH values. As illustrated in the inset, V_{TH} also appears to have a linear dependence on the pH value and shows a voltage sensitivity of 17 mV/pH. In general, the characteristics of the *I–V* curves indicate that our LGAA Si NW FET device exhibits stable FET properties, taking into account the very reproducible and stable pH response of devices covered by 20 nm SiO_2 contacting with a liquid. This is particularly crucial for biosensing applications.

Modeling results support experimentally obtained data using the *I–V* characterization method of liquid–solid interface properties in different pH solutions. **Figure** 3A shows the results of calculations of the potential energy redistribution in a Si/SiO_2/liquid structure at a value of −1 V, obtained using Next Nano software.[23] In Figure 3B, a surface potential drop is shown as a function of the distance calculated using Next Nano software for different pH values (6.0, 6.5, 7.0, 7.5, and 8.0) of PBS solutions.

The higher the pH value is, the stronger the value of the electric field near the liquid–solid interface. Such electric fields influence the mobility of ions in the solution near the interface by restricting their transport to the small region close to the SiO_2 layer.

To gain a better understanding of the ionic behavior at the liquid–solid interface in our LGAA device, capacitance-voltage (C-V) measurements were performed using flat SiO_2/Si/Al samples. A 20 nm SiO_2 flat layer was fabricated with the same thickness as the 20 nm SiO_2 layer, covering NW in the GAA FET structures. C–V characteristics were measured in 10mM PBS solutions with a different pH values (**Figure** 4A) at a frequency of 1kHz. The capacitance shifted to higher voltages with increasing pH values. To confirm the accuracy and repeatability of the results, the C–V measurements were repeated with increased and decreased pH solutions. The shifts due to the change in pH are characterized by voltage variations at a constant value of capacitance of C = 40 nF. A voltage shift at C = 40 nF was obtained at

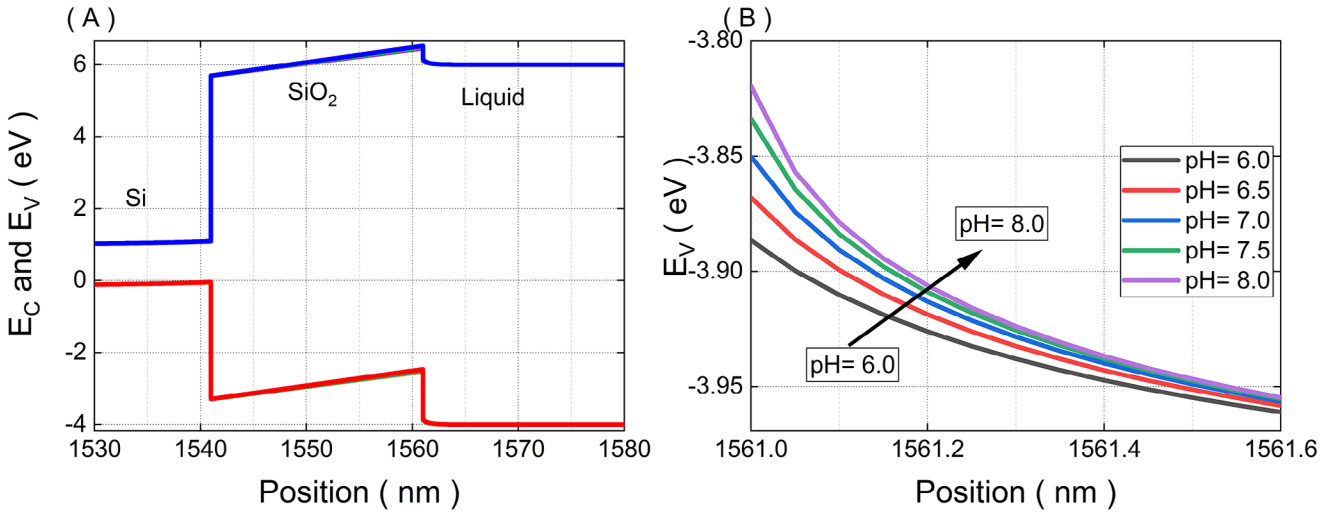

Figure 3. A) Potential energy redistribution is a Si/SiO_2/ liquid structure at the value of −1 V, calculated using Next Nano software for a 10 mM PBS solution with a content of 140 mM NaCl for different pH solutions: 6.0, 6.5, 7.0, 7.5, and 8.0. B) Enlarged part of the valence band potential redistribution at the solid-liquid interface, reflecting surface potential drop as a function of distance calculated using Next Nano software for different pH solutions: 6.0, 6.5, 7.0, 7.5, and 8.0.

≈16 mV/pH in 10 mM PBS solutions. The sensitivity of the capacitance curve to the pH change can be explained by the change in surface charge in the different pH solutions when increasing the pH value and the change in energy barrier at the liquid–solid interface.[24] The flat-band voltage V_{FB} variation in different pH solutions is illustrated in Figure 4B, which was calculated from the Mott–Schottky plot obtained using the C–V data.[25] The flat-band voltage shows a linear dependence on pH and demonstrates a sensitivity of ≈16 mV/pH, which is in agreement with the voltage shift result shown in Figure 2A. The stable shift of the flat-band voltage demonstrated the sensitive response of the sample to the change in pH values. It should be noted that previously in $MgCl_2$ solutions of different concentrations, a non-monotonous dependence on the concentration was obtained due to the inversion charge effect near the nanowire surface.[26] This was explained by the competitive mechanism for the attachment of ions at the liquid–solid interface, which is critical in biomolecule signal detection and analysis. In the case of PBS solutions of different pH values, very well-resolved non-monotonous behavior near the minimum capacitance was registered (Figure 4C). The minimum capacitance point determined from these data decreases with an increase in pH and subsequently grows after a value of pH 6.8 (Figure 4D). Models developed previously consider that inversion charge at liquid–solid interface can be registered in divalent and higher changed states ion solutions.[27–29] However, our results demonstrated that in the case of monovalent solutions, including NaCl as a main component in water solution, there is also a competitive mechanism resulting in the charge inversion at the liquid/solid interface.

To further analyze the ion response and carrier transport behavior around the nanowire, low-frequency noise spectroscopy was applied to study dynamic properties in different pH solutions. **Figure** 5A shows noise spectra measured at a small drain voltage of V_{DS} = −0.1 V and at an open channel condition of V_{LG} = −0.5 V. In our LGAA Si NW FET device, the majority of the noise spectrum within the 1 Hz to 10^4 Hz low-frequency region is represented by the *1/f* flicker noise, which is shown as a linear dependence in the low-frequency region in Figure 5A. The normalized spectral density of the current fluctuation value $S_I(f)/I^2$ at a frequency of 10 Hz is shown in Figure 5B for 10 mM PBS of different pH solutions, revealing a clear decrease in noise power density as the pH increases. As shown in Figure 5B, $S_I(f)/I^2$ linearly decreased from 1.5×10^{-7} Hz^{-1} to 9×10^{-8} Hz^{-1} as the pH changed from 6.0 to 8.0. The results indicate that a lower noise level can be reached in the high pH solution (≈7.4 pH) compared to pH 6.0, which is a consequence of the ion transport behavior change at the liquid-solid surface.

To gain a better understanding of the liquid–solid interface interactions, the equivalent input-referred noise, S_U, in different solutions was calculated and plotted in Figure 5C, which shows the equivalent input noise at a low frequency of 10 Hz in the solution pH range from 6.0 to 8.0. The input-referred noise in the solutions of different pH values indicated that ion transport caused current fluctuation around the NW (Figure 5C). For the case of insensitivity to the surface phenomena in liquid the behavior should be independent of pH value, i.e. horizontal line. However, our LGAA FETs demonstrate a decreasing S_U until pH 6.6, followed by a transformation region including the charge inversion point pH 6.8 obtained from C-V characteristics (Figure 4C) and again a decreased slope starting from pH 7.0. An increase in pH results in a decrease in positively charged hydrogen ions and their interaction with the surface, followed by increased values of negatively charged OH^- ions of large size. The Hooge parameter is usually used to compare the quality of different materials and device structures, operating in different environments, including liquids.[26,30] The dimensionless Hooge parameter, α_H, obtained using the flicker component of noise spectra measured in different pH solutions (Figure 5D) is calculated as follows:

$$\alpha_{\mathrm{H}}(\mathrm{f}) = \frac{\mathrm{S_I(f)}}{\mathrm{V_{DS}^2}} \frac{\mathrm{fL^2R}}{\mathrm{q}\mu_{\mathrm{p}}} \quad (1)$$

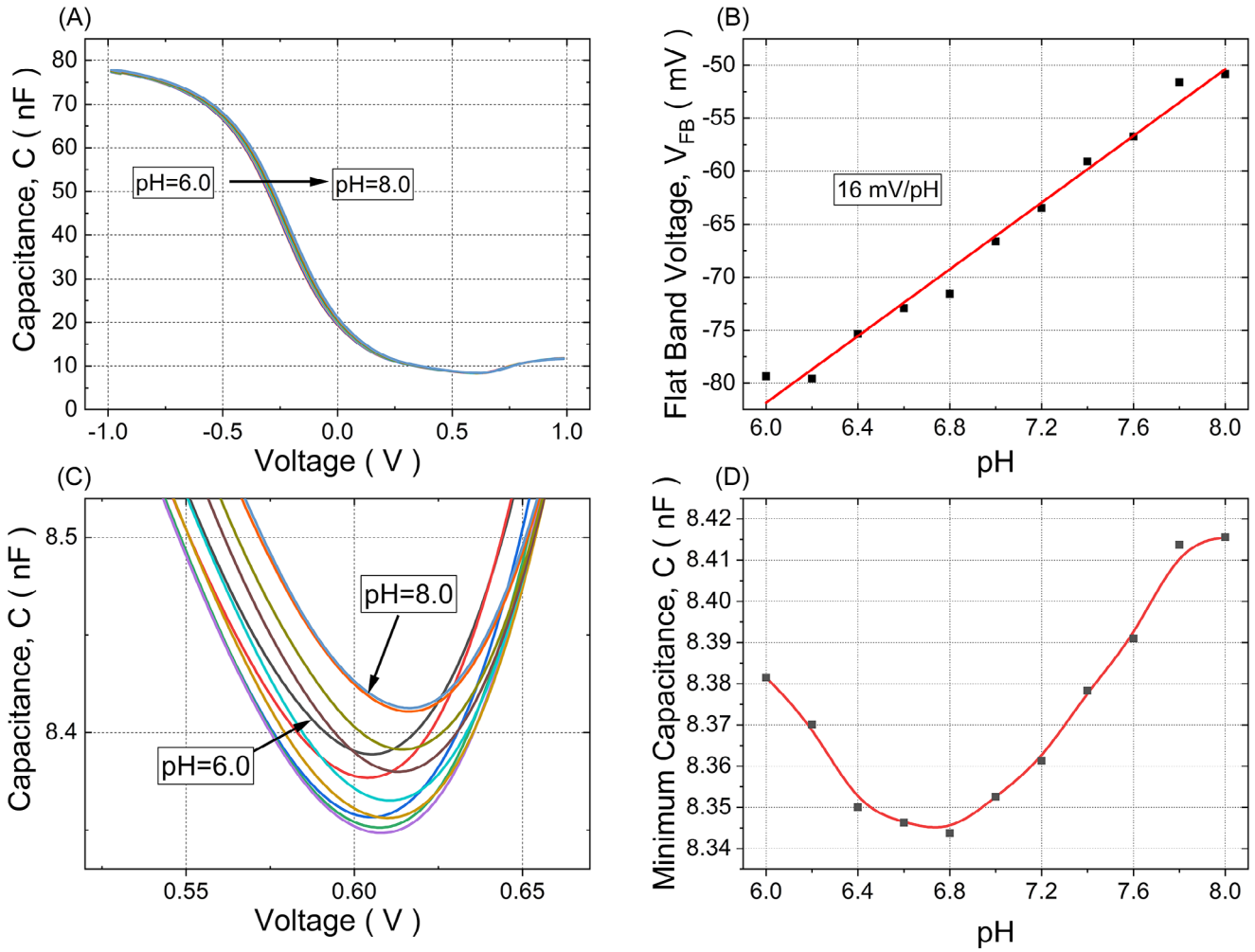

Figure 4. A) C–V characteristics measured in different pH values, with an incremental increase of 0.2 in 10 mM PBS solutions; B) V_{FB} variations in different pH solutions; C) characteristics obtained near minimum capacitance in different pH solutions; D) minimum capacitance plotted as a function of pH value.

where L is the nanochannel length, R is the resistance of the device, q is the elementary charge, and μ_p is the hole mobility.

It should be emphasized, that α_H values at the level of 1×10^{-3} obtained for our liquid-gated devices reflect the high-quality performance of FETs.[30,31]

Moreover, the low-frequency noise in our device is strongly controlled by liquid-gate voltage. To shed light on the influence of V_{LG} control on low-frequency noise, the S_V spectra at different gate voltages were measured. **Figure** 6A shows the noise response measured at different V_{LG} voltages in a pH 7.4 PBS solution under $V_{DS} = -0.1$ V, with gate voltage ranging from −0.30 to −0.58 V, which was measured with an incremental increase of 0.02 V. In the low-frequency range, the linear part typical for flicker noise in $1/f^{\gamma}$ behavior is resolved in the noise spectra. In addition, the generation–recombination (GR) noise component is recorded with a clear maximum in all noise spectra.

The GR shifts to a lower frequency range with an increase in liquid gate voltage. The maximum frequency, f_{max}, corresponding to GR maximum can be used to determine the characteristic time, τ, by the following relation:

$$f_{\max} = \frac{1}{2\pi\tau} \tag{2}$$

The characteristic time constant increases with liquid-gate voltage (Figure 6B). The results of Figure 6B confirm that the variation of the noise determined by ion dynamic processes can be gate-controlled in the FET. Furthermore, Figure 6C shows that the normalized current spectral density, $S_I(f)/I^2$, obtained at a frequency of 10 Hz demonstrates a decreasing dependence on V_{LG}.

Moreover, input-referred noise, S_U (Figure 6D), demonstrates that fluctuations at the liquid–solid interface can be controlled by V_{LG} voltage. In contrast to the constant S_U values typically not dependent V_{LG} obtained for large areas of Si NW FETs, S_U decreases with increasing liquid-gate voltage in small area GAA liquid-gated devices in the subthreshold and above-threshold regions. This confirms that the noise level is determined by fluctu-

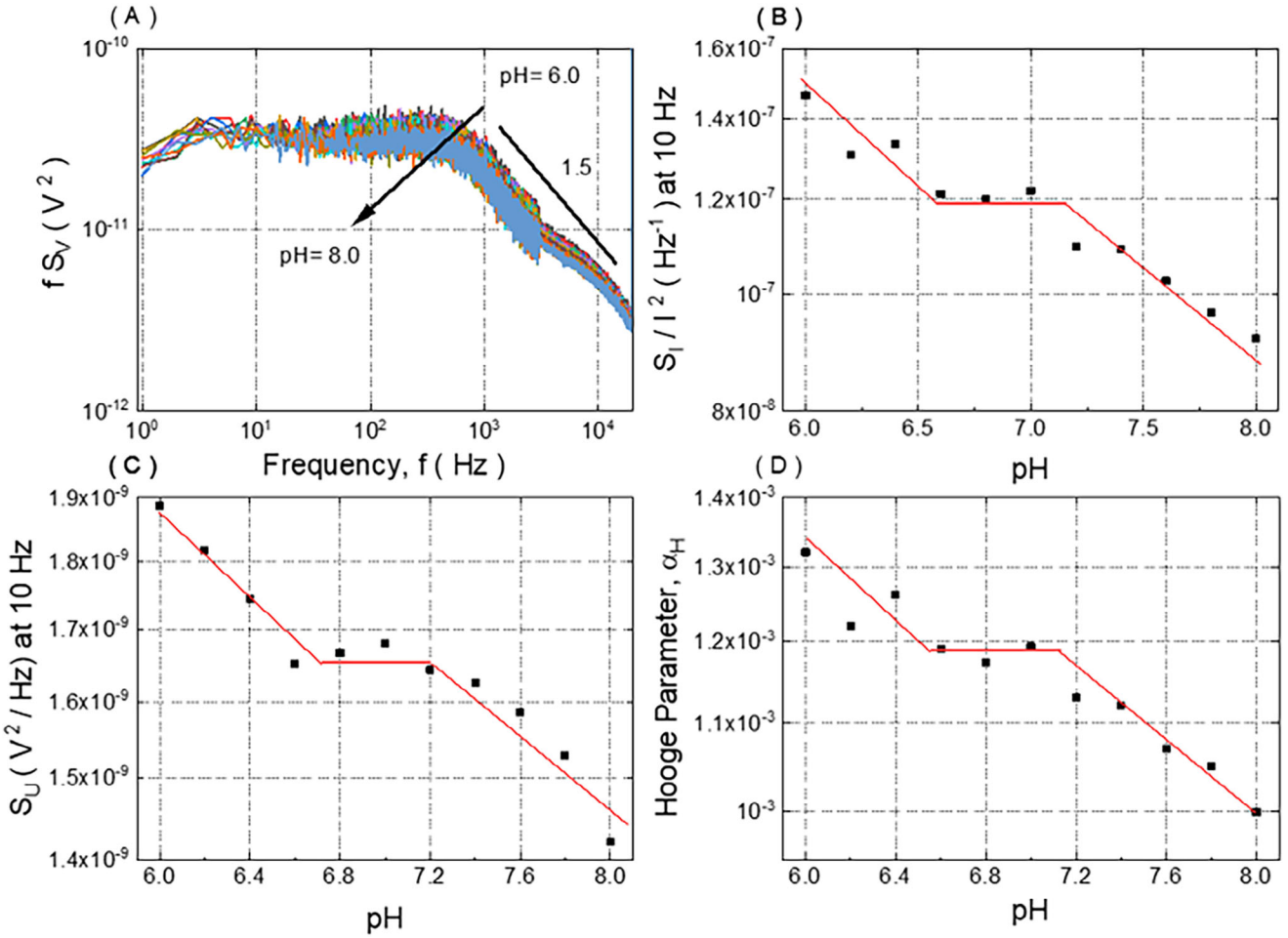

Figure 5. A) Low-frequency noise spectra multiplied by the frequency for a GAA NW FET in 10 mM PBS solutions with different pH values, with an incremental increase of 0.2, obtained at $V_{DS} = -0.1$ V and $V_{GS} = -0.5$ V; B) normalized spectral density of the current fluctuation value $S_I(f)/I^2$ at 10 Hz frequency for different pH solutions; C) equivalent input noise, S_U, at 10 Hz in solutions of different pH values; D) dimensionless Hooge parameter, α_H, in solutions with different pH values.

ation processes at the surface contacting with a liquid and corresponds to specific ion fluctuation processes at the liquid–solid interface.[13,26] Thus, the results demonstrate that ion-related fluctuations can be controlled by voltage on the gate and considerably suppressed in FETs with nano-channel in contrast to large-area FET devices. Actually, choosing the correct NW FETs' working point in with the physiologically-relevant solutions with pH value of 7.4 allows us for ultrasensitive detection of amyloid-beta biomarkers.[18] Obtained in this work sensitivity at the concentration of 20 fM is very promising for the predictable diagnostics and detection of Alzheimer's disease at the earliest stage.

It is also important to gain a deep understanding of the origin of noise and the contribution of generated components at zero drain-source voltages. In liquid systems, liquid noise can also be an informative parameter that reflects valuable data about the characteristics of ion layer formation around the nanowire and processes at the liquid–electrode interface. To further analyze the liquid system noise, the voltage noise spectral densities with different drain voltages are shown in **Figure** 7A at $V_{LG} = -0.5$ V. The results indicate that in the low-frequency region, the S_V level decreases as V_{DS} decreases.

Furthermore, the decreasing tendency is obtained in the normalized noise spectral density of the current fluctuation S_I/I^2 value at 10 Hz, as shown in Figure 7B. Figure 7B shows that the S_I/I^2 value significantly depends on V_{DS}, even in linear mode operation. For the case of noise determined mainly by dynamic processes in the channel, there is no such dependence and the S_I/I^2 value does not change. The strong dependence of S_I/I^2 on V_{DS} confirms that the noise presented here is generated by fluctuations at the SiO_2/electrolyte interface, i.e. ion charge fluctuations near this interface in liquid environments. Figure 7B also shows the relationship between V_{DS} and S_I/I^2 at 10 Hz for solutions with different pH values. In addition, linear behavior is obtained, as shown in Figure 7B, indicating that the liquid noise for the ion layer at the liquid–solid interface can be presented as an S_I/I^2 linear fitting value at $V_{DS} = 0$ V. In general, the voltage power spectral density decreased linearly with pH, which is consistent with the results shown in Figure 5. In Figure 7B, extrapolation lines to $V_{DS} = 0$V voltage

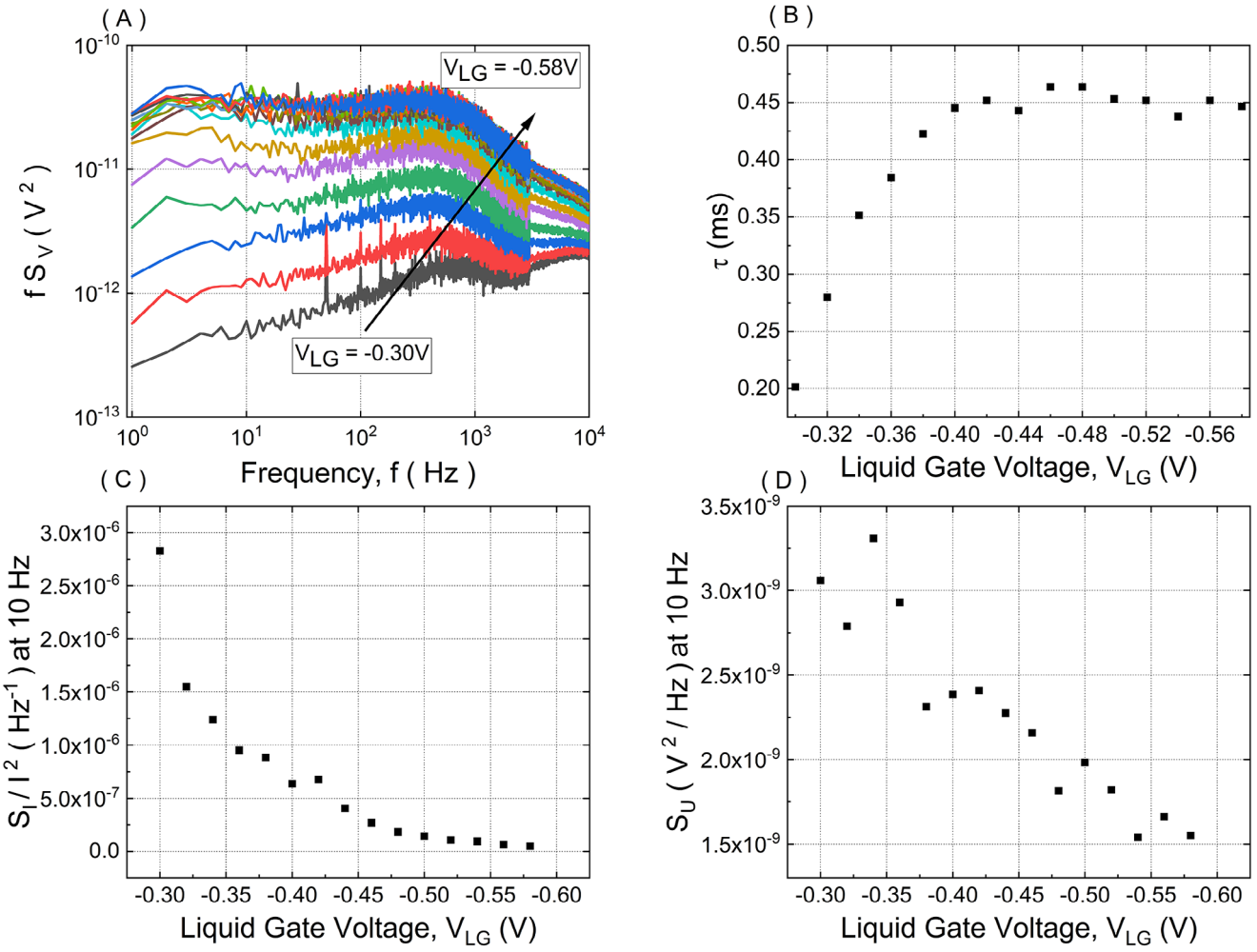

Figure 6. A) Typical noise spectra multiplied by the frequency measured for LG NW FET at different V_{LG} in a pH = 7.4 10 mM PBS solution under V_{DS} = −0.1 V; B) characteristic time constant corresponding to GR noise component of spectra shown in Figure 6A, extracted as a function of liquid-gate voltage; C) normalized noise spectral density of current fluctuation S_I/I^2 obtained at a frequency of 10 Hz; D) input-referred noise, S_U, obtained at a frequency of 10 Hz.

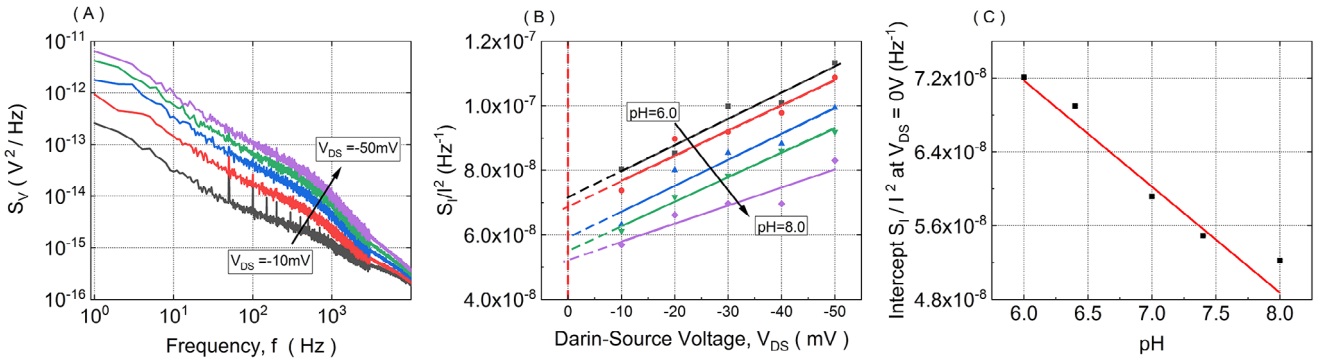

Figure 7. A) Voltage noise spectral densities of LG NW FETs at V_{LG} = −0.5V and different V_{DS} voltages(mV): = 10, 20, 30, 40, and 60; B) normalized noise spectral density of the current fluctuation S_I/I^2 value at 10 Hz and V_{LG} = −0.5 V as a function of drain-source voltage in solutions of different pH values: 6.0; 6.4; 7.0; 7.4; 8.0; C) dependence of the extrapolated S_I/I^2 value to 0 V_{DS} value shown for different pH values.

enable the ion behavior to be analyzed for the ideal case, i.e., without the influence of V_{DS} voltage. The obtained results are shown in Figure 7C, for the S_I/I^2 values plotted for different pH values.

The Lorentzian component in the noise spectra demonstrates high-frequency decay with a slope close to 1.5 (Figures 5A and 7A), which is characteristic of diffusion processes in the structure. The time constant of generation-recombination (GR) noise is determined by the diffusion time charges from the point of their appearance to the point of neutralization. Thus, the nature of such noise is related to the diffusion processes in the double-layer capacitance of the electrolyte in the LGAA FETs. It should be noted that the presence of diffusion noise confirms that the main noise source is related to fluctuating processes in liquids near SiO_2 layer covering NW. The dependence of the time constant GR of the noise component on the gate voltage V_{LG}, presented in Figure 6B, characterizes the mobility of charge carriers in the transient liquid layer. i.e., the diffusion time of charge carriers in this layer. The mobility of carriers in the transient layer decreases with increasing $|V_{LG}|$ voltage as a result of potential redistribution across the structure. This is confirmed by Figure 3B, where one can see that the interface layer becomes thinner and denser. As a result, the mobility of charge carriers in the interface layer decreases, and, accordingly, the diffusion time increases.

A specific tiny noise signal variation can also effectively reflect the ion transport behavior at the liquid–solid interface. The dependence of the liquid noise as a function of the pH value (Figure 5C) is in good agreement with the inversion (Figure 4D) of minimum capacitance registered in monovalent solutions in C-V characteristics, which strongly supports the noise results obtained. Results of the study of charge fluctuations due to ion transport provide useful signal information, which should be used to detect very small signals from biological molecules. In general, liquid noise can be regarded as a reflection method of the ion behavior in our LGAA Si NW FET device, which is critical for further signal analysis of ions, biomolecules, and changes of pH imparing human health.

3. Conclusion

In summary, we fabricated high-quality LGAA NW FET sensors and performed in-depth research on the analysis of noise spectroscopy in liquid–solid interfaces for adjusted physiological solutions with different pH values. *I–V* characteristics of the LGAA NW FET devices are in good agreement with modeling results and demonstrate reproducible pH sensitivity and high-quality device performance. Capacitance–voltage features reflect the competitive mechanisms of ions approaching the LGAA NW FET structure and the inversion effect in monovalent solutions. More detailed information was provided using the data of low-frequency noise spectroscopy characterization, which was performed under different voltage regimes and pH conditions. The results of the noise measurements demonstrate a powerful method for obtaining an in-depth understanding of ion transport behavior in liquids using NW FETs as advanced transducers. Dimensionless Hooge parameter values at the level of 10^{-3} reflect the high quality of LGAA NW FETs. The characterization of low-frequency noise properties of FETs in ion solutions at different applied gate voltages proved that the device regimes can be effectively controlled for biosensing applications. Furthermore, the ion transport behavior in our LGAA NW FETs is analyzed using normalized S_I/I^2 and input-referred noise data, reflecting the physical origin of noise in the device structures to be determined by liquid fluctuations. Analysis of input-referred noise, $S_{U,}$ of LGAA FETs demonstrates that the main source of noise is not related to nanotransistor device structure, but is determined by ion processes and thickness of the transformation layer in pH liquids. With the increase of liquid gate voltage, $V_{LG,}$ and increase of pH from 6.0 to 8.0 value S_U decreases. The fact reflects improved optimal conditions for the detection of very small biological signals. However, V_{LG} should be selected taking into account the thin-film dielectric layer protecting NW from direct contact with a liquid and conditions to prevent leakage current. Therefore V_{LG} should be selected just above the threshold voltage for the NW FET sensor. The results obtained should be taken into account when analyzing biological liquids and the selection of optimal parameters and working regimes for monitoring pH of bodily fluids and biomedical diagnostics as well as post-treatment stages toward restoring the healthy state.

4. Experimental Section

High-quality LGAA Si NW FET devices were fabricated using silicon-on-insulator (SOI) wafers, with $N_A = 10^{15}$ cm^{-3} doping of 50 nm Si on 150 nm SiO_2 box layer. Fabrication was based on a top-down approach. For the fabrication process, a full RCA cleaning process was first performed to guarantee SOI wafers with a high-quality surface. The top SiO_2 layer was then grown at a temperature of 900 °C to form a SiO_2 hard mask for patterning of the Si layer of SOI wafers to nanowire structures. After alignment markers were formed by reactive-ion etching (RIE), the nanowire structures were transformed from a hard mask to a Si layer using electron-beam lithography (EBL) and wet etching with a tetramethylammonium hydroxide (TMAH) solution at 80 °C. Boron ion implantation was introduced to form the drain and source ohmic contacts using a source with power energy of 6 keV and a dose of 10^{15} cm^{-2}, followed by rapid thermal processing (RTP) for 5 s at 1000 °C. A gate dielectric layer was grown by thermal oxidation with a thickness of 20 nm. The LGAA structure was etched using a buffered oxide etching solution for box-layer etching. To obtain ohmic contact, 5 nm Ti and 200 nm Al were thermally evaporated and lift-off was performed in acetone for 1 h to form the feedline and contact pad. RTP was then performed for 10 min at 450 °C for metal annealing. The passivation protection process was performed using a two-layer resist structure: PI 2545 and AZ-nlof 2020 by spin coating. After photolithographically patterned AZ-nlof 2020 layer, a 2 ×10 μm^2 window was formed over the NW for contacting with a solution. Finally, the encapsulation process was performed using polydimethylsiloxane (PDMS) after wire bonding, and the device was fully prepared for further experiments in a physiological-like solution containing 10 mM PBS, 138 mM NaCl, and 2.7 mM KCl with a total ionic strength of 150 mM.

Characterizations: All the measurements were performed in a Faraday cage using a specially designed measurement system. The typical *I–V* characteristics were measured using a Keithley 2400 and Keithley 2430 combination system, where the Ag/AgCl (diameter ≈1 mm and length ≈2 mm) reference electrode was immersed in the chosen solutions (≈100 µL), and the liquid gate was created over the sample nanowire opened window. Capacitance–voltage measurements were performed with a HIOKI 3532-50 LCR impedance meter, while 1k Hz AC voltage was applied by the Ag/AgCl electrode in the liquid gate. Noise spectroscopy was performed using an in-house-developed ultralow-noise measurement setup (PyFANS), combined with a power supply system comprising a rechargeable battery, amplifier system, a data analysis system, and a low-frequency

noise amplification cascade system, which enabled high-quality noise spectrum recording.

Statistical Analysis: For objective and effective statistical analysis, it is crucial to address the separation of valuable noise signals from various noises that may be recorded during the measurements. It is essential to avoid the impact of thermal noise on the results before processing any initial noise data $S_v(f)$. Attention should therefore be paid to the thermal noise $S_{Thermal}(f)$, with the equation given by:

$$S_{V\_Thermal}(f) = 4kTR_{eq} \tag{3}$$

where k represents the Boltzmann constant, and T is the non-zero temperature. To eliminate the noise arising from the thermal excitation of the charge carriers, the residual noise is expressed in the Equation (4).

$$S_{v,real}(f) = S_v(f) - 4KTR_{eq} \tag{4}$$

To investigate the fluctuation of current spectral density under various conditions at a frequency of 10 Hz, Equation (5) was used:

$$S_I(f) = \frac{S_{v,real}(f)}{R_{eq}^2}\left[\frac{1}{1+\left(\frac{f}{f_0}\right)^2}\right]^{-1} \tag{5}$$

where f_0 represents the corner frequency, originating from the parasitic capacitance of the preamplifier input.

The Lorentzian shape, closely related to the two-level RTS spectra, can be expressed using the following equation:

$$S_I(f) = \frac{4\Delta I^2}{(\tau_c+\tau_e)\left[\left(\frac{1}{\tau_c}+\frac{1}{\tau_e}\right)^2+(2\pi f)^2\right]} \tag{6}$$

where the ΔI represents the change in I_{DS} arising from the capture and emission processes of carriers by a single trap near the Si/SiO_2 interface.

Supporting Information

Supporting Information is available from the Wiley Online Library or from the author.

Acknowledgements

Y.Z. and H.L. are very grateful for the research grants received from the China Scholarship Council (CSC). The authors would also like to thank the technical staff of the Helmholtz Nano Facility (HNF) of Forschungszentrum Jülich for their assistance in fabricating the sensor devices. M.P. is grateful for a research grant from the Helmholtz Initiative and Networking Fund.

Conflict of Interest

The authors declare no conflict of interest.

Data Availability Statement

The data that support the findings of this study are available from the corresponding author upon reasonable request.

Keywords

FET biosensor, GAA nanowire, interface noise, low-frequency noise spectroscopy, pH sensing

Received: July 9, 2025
Published online: August 25, 2025

[1] D. P. Tran, T. T. T. Pham, B. Wolfrum, A. Offenhausser, B. Thierry, *Materials* **2018**, *11*, 785.
[2] Q. Li, N. Lu, L. Wang, C. Fan, *Small Methods* **2018**, *2*, 1700263.
[3] J. Hahm, C. M. Lieber, *Nano Lett.* **2003**, *4*, 51.
[4] E. Stern, J. F. Klemic, D. A. Routenberg, P. N. Wyrembak, D. B. Turner-Evans, A. D. Hamilton, D. A. Lavan, T. M. Fahmz, M. A. Reed, *Nature* **2007**, *445*, 519.
[5] B. R. Li, C. W. Chen, W. L. Yang, T. Y. Lin, C. Y. Pan, Y. T. Chen, *Biosens. Bioelectron.* **2013**, *45*, 252.
[6] D. Singh, G. C. Patil, *IEEE Sens. J.* **2020**, *20*, 13269.
[7] X. P. Gao, G. Zheng, C. M. Lieber, *Nano Lett.* **2010**, *10*, 547.
[8] C. Wei, Y. Z. Xiong, X. Zhou, *IEEE Trans. Electron Devices* **2009**, *56*, 2800.
[9] Y. Zhang, N. Boichuk, D. Pustovyi, V. Chekubasheva, H. Long, M. Petrychuk, S. Vitusevich, *Adv. Electronic Mater.* **2024**, *10*, 2300855.
[10] G. Yamahata, K. Nishiguchi, A. Fujiwara, *Nat. Commun.* **2014**, *5*, 5038.
[11] J. Li, S. Pud, M. Petrychuk, A. Offenhausser, S. Vitusevich, *Nano Lett.* **2014**, *14*, 3504.
[12] Y. Kutovyi, I. Zadorozhnyi, H. Hlukhova, V. Handziuk, M. Petrychuk, A. Ivanchuk, S. Vitusevich, *Nanotechnology* **2018**, *29*, 175202.
[13] Y. Guo, D. Pustovyi, Y. Kutovyi, N. Boichuk, M. Petrychuk, Y. Zhang, S. Vitusevich, *Adv. Mater. Interfaces* **2022**, *9*, 2201142.
[14] S. Vitusevich, I. Zadorozhnyi, **2017**, *32*, 043002.
[15] G. He, J. Li, H. Ci, C. Qi, X. Guo, *Angew. Chem., Int. Ed.* **2016**, *55*, 9036.
[16] S. Vernick, S. M. Trocchia, S. B. Warren, E. F. Young, D. Bouilly, R. L. Gonzalez, C. Nuckolls, K. l. Shepard, *Nat. Commun.* **2017**, *8*, 15450.
[17] W. Liu, J. Li, Y. Xu, D. Yin, X. Zhu, H. Fu, X. Su, X. Guo, *Adv. Sci.* **2021**, *8*, 2101383.
[18] Y. Kutovyi, H. Hlukhova, N. Boichuk, M. Menger, A. Offenhausser, S. Vitusevich, *Biosens. Bioelectron.* **2020**, *154*, 112053.
[19] Y. Kutovyi, V. Piatnytsia, N. Boichuk, I. Zadorozhnyi, J. Li, M. Petrychuk, S. Vitusevich, *Adv. Electronic Mater.* **2021**, *7*, 2000858.
[20] A. U. Alam, Y. Qin, S. Nambiar, J. T. W. Yeow, M. M. R. Howlader, N. X. Hu, M. J. Deen, *Prog. Mater. Sci.* **2018**, *96*, 174.
[21] H. Ren, K. Liang, D. Li, Y. Chen, Y. Tang, Y. Wang, F. Li, G. Liu, B. Zhu, *Adv. Sensor Res.* **2023**, *2*, 2200098.
[22] M. Michaelis, N. Hildebrand, R. H. Meißner, N. Wurzler, Z. Li, J. D. Hirst, A. Micsonai, J. Kardos, M. Delle Piane, L. Colombi Ciacchi, *J. Phys. Chem. B* **2019**, *123*, 6694
[23] S. Birner, C. Uhl, M. Bayer, P. Vogl, *J.Phys.:Conf.Ser* **2008**, *107*, 012002
[24] A. Prakash, A. Das, S. Maikap, C. S. Lai, 9th IEEE Conference on Nanotechnology (IEEE-NANO), IEEE, New York **2009**.
[25] K. Gelderman, L. Lee, S. W. Donne, *J. Chem. Education* **2007**, *84*, 685.
[26] Y. Zhang, N. Boichuk, D. Pustovyi, V. Chekubasheva, H. Long, M. Petrychuk, S. Vitusevich, *Adv. Mater. Interfaces* **2023**, *10*, 2300585.
[27] J. Wu, *Chem. Rev.* **2022**, *122*, 10821.
[28] S. X. Li, W. Guan, B. Weiner, M. A. Reed, *Nano Lett.* **2015**, *15*, 5046.
[29] K. Besteman, M. A. Zevenbergen, S. G. Lemay, *Phys. Rev. E Stat. Nonlin Soft Matter Phys.* **2005**, *72*, 061501.
[30] F. H. Hooge, *Phys. B* **1972**, *60*, 130-144.
[31] I. Zadorozhnyi, Y. Kutovyi, H. Hlukhova, M. Petrychuk, S. Vitusevich, in Proc. of the 2017 International Conf. on Noise and Fluctuations (ICNF), IEEE, New York **2017**.